Thermal Motions in Bacteriorhodopsin at Different Hydration Levels Studied by Neutron Scattering: Correlation with Kinetics and Light-Induced Conformational Changes

Ursula Lehnert,*§ Valérie Réat,* Martin Weik,* Giuseppe Zaccaï,*§ and Claude Pfister*#
*Institut de Biologie Structurale, 38027 Grenoble Cedex 1, France, #Université J. Fourier, BP 53, 38041 Grenoble Cedex 9, France, and §Institut Laue-Langevin, BP 156X, 38042 Grenoble Cedex 9, France

ABSTRACT Bacteriorhodopsin (BR) is a transmembrane protein in the purple membrane (PM) of *Halobacterium salinarum*. Its function as a light-driven proton pump is associated with a cycle of photointermediates which is strongly hydration-dependent. Using energy-resolved neutron scattering, we analyzed the thermal motions (in the nanosecond-to-picosecond time range) in PM at different hydration levels. Two main populations of motions were found that responded differently to water binding. Striking correlations appeared between these "fast" motions and the "slower" kinetic constants (in the millisecond time range) of relaxations and conformational changes occurring during the photocycle.

INTRODUCTION

Bacteriorhodopsin (BR) is the only protein in the purple membrane (PM) patches of the plasma membrane of the archaeon *Halobacterium salinarum*. It functions as a light-activated proton pump. After absorption of a photon by its bound chromophore, retinal, BR goes through several sequential photointermediates and finally returns to its initial state. These are defined by the wavelength of maximal absorbance in nm: BR_{568}, J_{610}, K_{590}, L_{550}, M_{412}, N_{550}, and O_{640}; the M intermediate is the most stable, and corresponds to an irreversible transition between two steps, M_1 and M_2. During this photocycle, a proton is released to the extracellular medium during the L-to-M transition, and another one bound from the intracellular medium between N and O. The influence of hydration on the kinetics of appearance and decay of the photointermediates has been analyzed by visible and FTIR spectroscopy (Korenstein and Hess, 1977; Váró and Keszthelyi, 1983; Váró and Lanyi, 1991a; Thiedemann et al., 1992). In fully hydrated samples at room temperature, photoexcited BR goes through all the intermediates of its photocycle. The steps $M_1 \Rightarrow M_2$ (irreversible) and $M_2 \Leftrightarrow N$ (reversible) are progressively slowed down when decreasing hydration, and the intermediates N and O are no longer detectable at low humidity (Váró and Lanyi, 1991a; Cao et al., 1991). In addition, structural changes in $M_1 \Rightarrow M_2$ and in $M_2 \Leftrightarrow N$ have been observed in the D96N mutant of BR to occur only at high hydration levels (Sass et al., 1997; Kamikubo et al., 1997; Weik et al., 1998). A direct study of proton pumping (or rather of charge movement) as a function of relative humidity has been published (Thiedemann et al., 1992), which also shows reduced kinetics at reduced relative humidity.

Incoherent elastic neutron scattering provides a means to quantify the amplitudes of H-atom motions in a molecule. In the corresponding picosecond-to-nanosecond time domain, the H-atoms reflect the motions of the chemical groups to which they are bound. As H-atoms are uniformly distributed in a biological sample, neutron experiments are a good experimental approach to study macromolecular dynamics (Smith, 1991). In the few proteins already studied by neutron scattering, dynamical transitions have been discovered, at 150–250 K, from a rigid harmonic to a softer nonharmonic regime (Doster et al., 1989; Ferrand et al., 1993; Andreani et al., 1995; Réat et al., 1997, 1998). Such transitions have also been characterized by various other experimental and theoretical methods (Loncharich and Brooks, 1990; Parak et al., 1990; Smith, 1991; Rasmussen et al., 1992; Cupane et al., 1993).

In fully hydrated BR, two populations of motions have been described by neutron scattering, associated with different dynamical transitions, at ~250 and 150 K, respectively (Ferrand et al., 1993; Réat et al., 1997); in completely dry BR, the dynamical transition at 250 K is absent (Ferrand et al., 1993; Réat et al., 1997); different characteristic times have been observed in quasielastic spectra, depending on hydration (Fitter et al., 1996, 1997b). A first qualitative correlation between BR function and thermal motions has been discussed by Ferrand et al. (1993) on the basis of a comparison between totally dry and fully hydrated samples, following a hypothesis that BR function required a soft and warm environment (Zaccaï, 1987). By using specific deuteration, Réat et al. (1998) have shown that the retinal pocket and extracellular half of BR of wet membranes are more "rigid" than the wet membranes globally, and discussed the implication of this dynamic heterogeneity for function.

Our goal in the present study was to investigate in detail how the different motions in BR depend on hydration to

Received for publication 28 January 1998 and in final form 5 July 1998.
Address reprint requests to Claude Pfister, Institut de Biologie Structurale, 41 Avenue des Martyrs, 38027 Grenoble Cedex 1, France. Tel.: 33-(0)4-76-88-95-70; Fax: 33-(0)4-76-88-54-94; E-mail: pfister@ibs.fr.

Valérie Réat's present address is Departments of Physics and Astronomy, University College London, Gower Street, London WC1E 6BT, England.

0006-3495/98/10/1945/08 $2.00

explore their relation to other hydration-dependent observations related to the photocycle and proton pumping. The results showed that different populations of motions respond differently to hydration, and a strong correlation between the parameters defining the "fast" motions and much "slower" kinetics of the intermediates of the photocycle and proton pumping events.

MATERIALS AND METHODS

Purple membrane preparation

Cultures of *Halobacterium salinarum* and purification of purple membranes were carried out as described by Oesterhelt and Krippahl (1983) and Oesterhelt and Stoeckenius (1974). Briefly, after culture and disruption of the plasma membrane by hypoosmotic shock was performed, the PM were fractionated on a sucrose density gradient, and the purple band was harvested, diluted in H_2O, and pelleted. Three washing steps in ^2H_2O by resuspension-centrifugation fully exchanged the water and labile hydrogen in the sample.

Equilibration in defined relative humidity values

The ^2H_2O-washed pellet (~150–180 mg BR, i.e., 200–250 mg PM) was layered in an aluminum sample holder (dimensions 4×3 cm^2, thickness 0.5 mm). Rapid, partial drying was achieved by placing the sample in a desiccator with silica gel at room temperature until the final ^2H_2O content reached ~0.5 mg/mg PM (measured by weighing). Final equilibration to the required hydration level was obtained by replacing the silica gel with a saturated solution of an appropriate salt in ^2H_2O; this precisely defined the relative humidity (r.h.). The salts were NaBr for 57% r.h., NaCl for 75% r.h., KCl for 86% r.h., and KNO_3 for 93% r.h. (O'Brien, 1948). The dry sample was obtained by complete desiccation over silica gel. Each equilibration proceeded for 5–7 days until the weight of the sample and sample holder did not vary by >0.5 mg. The sample holder was then sealed with an indium ring. The amount of water in the sample was estimated by weighing before and after complete drying over silica gel (results are in Fig. 5 *A*).

Elastic incoherent neutron scattering (EINS) and data acquisition

Neutrons are scattered by atomic nuclei. In an incoherent neutron scattering experiment, waves scattered by different nuclei do not interfere (Bée, 1988). The observed scattering intensity is the sum of intensities scattered by individual nuclei. It is analyzed by a neutron spectrometer, in terms of energy (frequency, ω) and momentum transfer (scattering vector, $\mathbf{Q}$), to provide $S(\mathbf{Q}, \omega)$. The scattering is elastic for $\omega = 0$, i.e., when, within the energy resolution of the spectrometer, there is no energy transfer between the incident and scattered neutrons. Elastic incoherent neutron scattering (EINS) reflects the displacements of individual atoms in the picosecond-to-nanosecond time range, depending on the energy resolution of the spectrometer. An energy broadening of the elastic peak corresponds to quasielastic scattering. It results from relaxation processes such as nonvibrational, diffusive motions or jumps between conformational substates. Vibrational motions give rise to inelastic scattering with peaks at distinct energy transfer values (Cusack, 1988) .

In biological macromolecules, ~50% of the atoms are hydrogens. The cross-section for incoherent scattering by these nuclei is much larger than the incoherent or coherent scattering of any of the other nuclei usually found in these molecules, or of ^2H. In the PM samples in ^2H_2O studied here, 90% of the total signal was due to incoherent scattering, of which ~63% was due to BR, 36% to lipids (10 lipids/BR, Grigorieff et al., 1996) and <1% to ^2H_2O.

In the present work, only the elastic incoherent neutron scattering was analyzed as a function of wavevector transfer $\mathbf{Q}$ and temperature. Its diminution as a function of increasing temperature reflects the onset of inelastic followed by quasielastic neutron scattering (Cusack, 1988). At a given temperature T, and in the Gaussian approximation, the $\mathbf{Q}$-dependence of $S_{inc}(\mathbf{Q}, \omega = 0, T)$ is written

$$S_{inc}(\mathbf{Q}, 0, T) = A \exp[-(1/6)\langle u^2\rangle \mathbf{Q}^2] \qquad (1)$$

where the mean-square amplitude $\langle u^2\rangle$ is dominated by the values of the ^1H-atoms in the sample, and A is a constant. The equation is appropriate for the full amplitude of atomic displacements during the time resolution of the experiment $\langle u^2\rangle = [R(t) - R(0)]^2$ and not to displacements from mean positions $[R(t) - R_{mean}]^2$, which is the value usually used in the Debye-Waller factor in crystallography ($\langle u^2\rangle/2 = [R(t) - R_{mean}]^2$ in the harmonic approximation). For the Gaussian approximation to be valid, either all ^1H-atoms must be dynamically equivalent and vibrate harmonically (Smith, 1991) or $\mathbf{Q}$ must be such that $\mathbf{Q}\sqrt{\langle u^2\rangle/2} < \approx 1$; this is similar to the relation between $\mathbf{Q}$ and the radius of gyration in the Guinier approximation for small angle scattering (Réat et al., 1997). In a small angle scattering experiment one measures the shape of a distribution of atoms. In an EINS experiment, one measures the shape of the distribution of an individual atom as it moves in the characteristic time interval of the spectrometer.

The experiments were performed on the IN13 backscattering spectrometer at the Institut Laue-Langevin (ILL; Grenoble, France). The detectors on the spectrometer cover a large $\mathbf{Q}$-range (from 0.3 Å^{-1} to 5.5 Å^{-1}; however, data were analyzed only up to 3.6 Å^{-1}, because of the statistically weak signal-to-noise ratio for higher angles).

The sample containers were placed in a cryostat, first taken to 20 K at a rate of 2 K/min; then the data were collected in 30-min accumulations per point, every 5 K from 20 to 320 K. At the end of the experiment, the sample container was weighed to ensure that no loss of water had occurred.

The raw data were corrected, at each $\mathbf{Q}$-value, for scattering by the empty sample container, detector response (by using a standard vanadium sample), and for transmission of the sample. Data for $\mathbf{Q}$-values corresponding to Bragg reflections of the sample-holder were discarded in the analysis. The energy resolution of the instrument is ≈ 10 μeV, corresponding to observable motions faster than 400 ps. Data were normalized, at each $\mathbf{Q}$-value, by the lowest temperature (20 K) data point. The results are therefore written as $S_{inc}(\mathbf{Q}, 0, T)/S_{inc}(\mathbf{Q}, 0, T_0)$. A linear fit of $\ln\{S_{inc}(\mathbf{Q}, 0, T)/S_{inc}(\mathbf{Q}, 0, T_0)\}$ as a function of $\mathbf{Q}^2$ was performed at each temperature, according to Eq. 1. The evaluation of errors on the slopes of the linear fit (and therefore on $\langle u^2\rangle$) assumed weighted statistical errors around each data point, and were calculated by the Marquardt-Levenberg algorithm in the Gnufit routine under Gnuplot (program version 3.5, copyright 1986–1993, Dartmouth University). The $\langle u^2\rangle$ values were then plotted as a function of absolute temperature T. In the harmonic case, $\langle u^2\rangle$ is linear with T, with a slope inversely proportional to the force constant governing the motion.

RESULTS AND DISCUSSION

Fig. 1 displays a typical result obtained in the complete $\mathbf{Q}$-range studied. It is especially clear at 300 K that the data cannot be fitted by a single straight line. Following Réat et al. (1997), we divided the $\mathbf{Q}$-range into two regions, the limit between the two ranges being taken at the value where a kink occurs in the plot of $\ln\{S_{inc}(\mathbf{Q}, 0, T)/S_{inc}(\mathbf{Q}, 0, T_0)\}$ as a function of $\mathbf{Q}^2$. We considered the two ranges separately. A mean-square amplitude $\langle u^2\rangle$ was calculated from the slope of each line (see Materials and Methods): a) The low $\mathbf{Q}$-range (0.3 Å^{-1} < $\mathbf{Q}$ < 1.8 Å^{-1}); here $\mathbf{Q}\sqrt{\langle u^2\rangle/2}$ ranges from 0.25 to 1.5. b) The high $\mathbf{Q}$-range (2.04 Å^{-1} < $\mathbf{Q}$ < 3.6 Å^{-1}); here $\mathbf{Q}\sqrt{\langle u^2\rangle/2}$ ranges from 1.0 to 1.8. The Gaussian approximation (see Materials and Methods) is

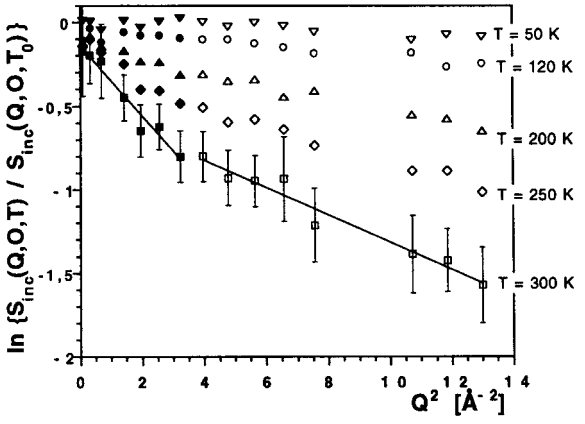

FIGURE 1 Intensities of elastically scattered neutrons by PM. The scattered intensities for each detector (each value of **Q**), corrected and normalized, are plotted as $\ln\{S(\mathbf{Q}, 0, T)/S(\mathbf{Q}, 0, T_0)\}$ as a function of $\mathbf{Q}^2$. The given data correspond to PM at 86% r.h. at five different temperatures. *Closed symbols:* data corresponding to the "low **Q**-range" in the analysis. *Open symbols:* data corresponding to the "high **Q**-range." Statistical errors are displayed for data obtained at 300 K. Solid lines are linear regressions on the data points; their slope gives the corresponding mean-square amplitudes $\langle u^2 \rangle$ (Eq. 1).

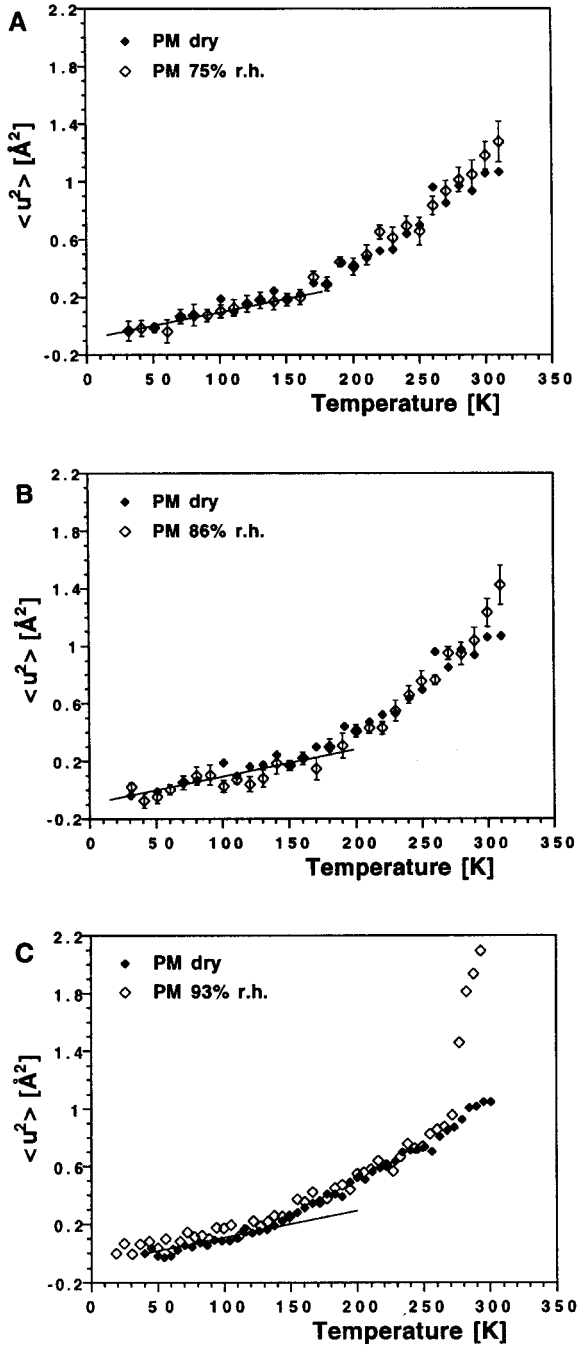

FIGURE 2 Mean-square amplitudes ($\langle u^2 \rangle$) of PM in the "low **Q**-range" as a function of temperature for four hydration conditions (0% r.h., 75% r.h., 86% r.h.: this work; 93% r.h.: data taken from experiments on IN10 at the ILL by Réat et al., 1997). 0% r.h.: closed symbols (data are reproduced in each figure); 75% r.h., 86% r.h., and 93% r.h.: open symbols for each hydration value (specified in the *inset*). *Solid line:* linear regression on the data points between 20 and 150 K (below the first dynamical transition), corresponding to harmonic vibrations. In (*A*) and (*B*), errors are drawn for the data on the hydrated samples; in (*C*), errors are of the size of the data points.

fully justified in the low **Q**-range, and reasonable for the high **Q**-range.

Fig. 2, *A* and *B* gives the variations of the mean-square amplitudes $\langle u^2 \rangle$ as a function of *T* for the low-**Q** region for 75% and 86% r.h., respectively, compared with the dry sample (0% r.h.). The data in Fig. 2 *C* (93% r.h. compared with 0%) were taken from the work of Réat et al. (1997), carried out in the same **Q**-range but on a different spectrometer at the ILL (IN10). Comparing data on IN10 and IN13 in the same **Q**-range has been justified by Réat et al. (1998), despite the difference in the energy resolution of the two instruments. This is also clear through the identity (within errors) of the dry PM data in Fig. 2, *A* and *B* on the one hand, and 2 *C* on the other. In this **Q**-range, "high-amplitude movements" (HA) dominate with mean-square amplitudes up to 2 Å^2. At temperatures below ≈150 K, in each case, the variation of $\langle u^2 \rangle$ with *T* can be fitted well by a straight line, reflecting the existence of harmonic motions. These movements are independent of the hydration level of the sample. A deviation from this line appears at ~150 K, reflecting the onset of nonharmonic movements. In the *T* range 150–270 K and under all the hydration conditions tested (including the dry sample), the $\langle u^2 \rangle$ values are very close, barely outside experimental errors; the corresponding motions were called "HA_1." Above 270 K, hydration affects $\langle u^2 \rangle$ amplitudes in a very minor way up to 86% r.h.; but, at 93% r.h., there is an abrupt rise in $\langle u^2 \rangle$ values; the corresponding motions were called "HA_2."

Fig. 3, *A–C* gives the variations of the mean-square amplitudes $\langle u^2 \rangle$ as a function of *T* in the high-**Q** range. The data for 57% r.h. were identical within errors with those of 0% r.h., and are not shown. In this **Q**-range, "small amplitude movements" (SA) of <1 Å^2 are dominant. At temperatures below 250 K in each case, the movements show harmonic behavior, and are not affected by hydration. Above 250 K, nonharmonic movements are triggered, with

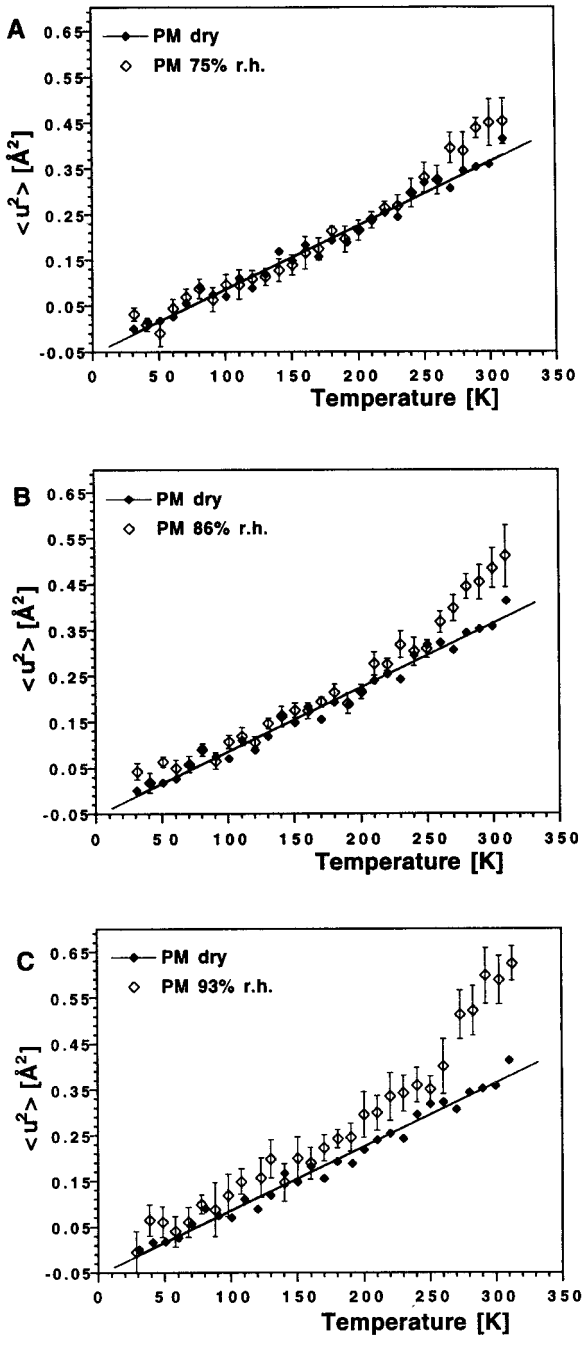

FIGURE 3 Mean-square amplitudes ($\langle u^2 \rangle$) of PM in the "high **Q**-range" as a function of temperature for four hydration conditions (0% r.h., 75% r.h., 86% r.h., 93% r.h.: this work). Same symbols as in Fig. 2.

deviations from the linear fit corresponding to harmonic movements increasing with hydration levels.

The quantitative influence of hydration on the mean-square amplitudes of the two populations of motions in the two different **Q**-ranges was calculated as follows: for HA_2 a linear fit was taken on the $\langle u^2 \rangle$ (T) data between 270 and 300 K after the second dynamical transition; for HA_1 a single linear fit was taken between 150 and 300 K (absence of dynamical transition at 270 K); for SA the linear fit was between 250 and 300 K (after the only dynamical transition). In Fig. 4 the relative difference of these slopes is shown, i.e., $\Delta\text{slope}/\text{slope}_{dry} = [\text{slope}_{r.h.} - \text{slope}_{dry}]/\text{slope}_{dry}$. The differences in the hydration-dependence of the SA and HA motions were clearly outside experimental error. For motions HA_1, the mean-square amplitudes were almost independent of hydration level; motions HA_2 appeared at a hydration level of 93% r.h.; the mean-square amplitudes of the SA motions increase regularly with increasing hydration level. These differences in behavior provided a self-consistent support for the hypothesis, discussed earlier by Réat et al. (1997), on the existence of two main populations of motions in the membrane.

The populations HA_1, HA_2, and SA were defined according to their mean-square amplitudes and dependence upon hydration. In a recent work, Fitter et al. (1997b) have defined two families of motions in PM ("faster" and "slower") according to different correlation times; these also were found to depend on temperature and hydration. The correspondence between the families defined by amplitude (this work) and by time or energy (in Fitter et al., 1997b) cannot be explored further without molecular dynamic simulations.

The influence of hydration on PM dynamics raises a number of questions.

1. As a function of relative humidity, how much water is bound to PM? The amount of water associated to PM at different r.h. values has been estimated by weight in this work. Values are concordant with data derived from Váró and Keszthelyi (1983) (Fig. 5*A*), which agree with preliminary NMR data (B. Bechinger, personal communication). The amount of associated water grows progressively up to 86% r.h., and then increases steeply.
2. As a function of hydration, what is the repartition of water molecules in the sample? Three hydration regions

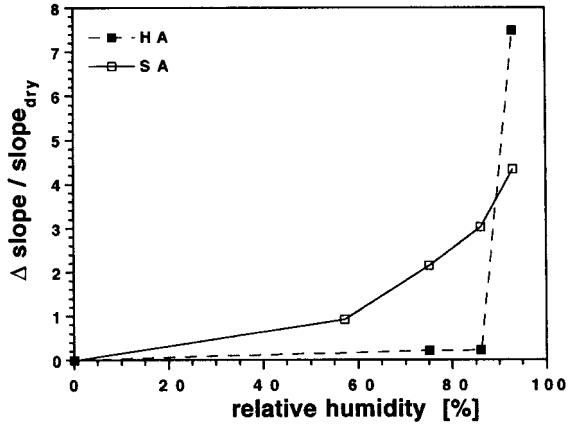

FIGURE 4 Influence of hydration on the mean-square amplitudes of motions in PM at 300 K. This was symbolized as $\Delta\text{slope}/\text{slope}_{dry}$, calculated as $(\text{slope}_{r.h.} - \text{slope}_{dry})/\text{slope}_{dry}$, in which $\text{slope}_{r.h.}$ and slope_{dry} are the slopes corresponding to a linear fit on the $\langle u^2 \rangle$ (T) data between 270 and 300 K for HA and between 250 and 300 K for SA for the hydrated and dry samples, respectively. *Open symbols and solid line:* influence of hydration on motions SA. *Closed symbols and dotted line:* influence of hydration on motions HA_1 and HA_2. Errors were of the size of the data symbols.

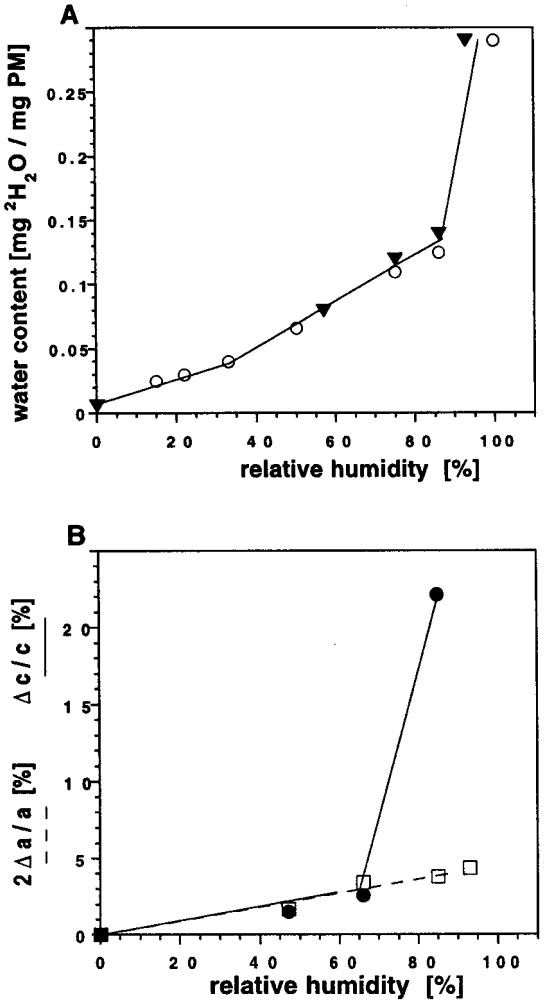

FIGURE 5 Structural characteristics of hydration of PM. (*A*) Water content of PM. *Triangles:* this work (derived from weight); *circles:* data derived from Váró and Keszthelyi, 1983, considering a relative contribution of lipids in PM of 25% w/w (Glaeser et al., 1985). (*B*) Lattice characteristics of PM (unpublished data obtained by Rogan and Zaccaï, 1981). *Squares:* relative increase in lipid area with increasing hydration, represented by twice the relative variation of the in-plane lattice parameter "a." *Circles:* swelling of the membrane stacks, represented by the relative variation of the stack lattice parameter "c." *Lines:* hand-drawn fits on the data to guide the eye.

have been identified in PM stacks: in the proton channel of BR, around the lipid headgroups, and between the membranes (Zaccaï and Gilmore, 1979; Rogan and Zaccaï, 1981; Papadopoulos et al., 1990). In hydrated PM, the number of bound water molecules estimated to be near the retinal and in the proton channel varies between 4 and 20 (Papadopoulos et al., 1990; Cao et al., 1991; Schulenberg et al., 1995; Rousso et al., 1997 and references therein; Pebay-Peyroula et al., 1997); it seems accepted that ~4 water molecules remain bound even under very low hydration conditions. The variation with relative humidity of the in-plane hexagonal unit cell dimension "a" is a measure of water associated with the lipid headgroups, leading to an increase of unit cell surface area; Fig. 5 *B* shows that this increase is roughly proportional to r.h. The variation with relative humidity of the lamellar period (parameter "c" in Fig. 5 *B*) reflects water association in the interbilayer space; it shows a steep increase above 66% r.h. (unpublished results of Rogan and Zaccaï). By rapidly cooling PM stacks at 93% r.h. down to 77 K, a decrease of the in-plane and lamellar lattice constants has been detected (Zaccaï, 1987), interpreted as a thermal contraction without loss of water on the lipid headgroups. With PM stacks at 100% r.h. and slower cooling rate, Lechner et al. (1998) found a more important dependence of the lamellar spacing below ~260–275 K, interpreted as a dehydration of the membrane and ice formation (Fitter et al., 1997b). In our conditions of hydration and cooling rate, Bragg peaks due to ice formation have not been detected. Lechner et al. (1994) found a significant dependence on r.h. in the translational diffusion of water in PM. It is low up to ~40% r.h. and increases strongly at ~93% r.h., while remaining much less than for bulk water. Rupley and Careri (1991) have suggested that the first part of the water adsorption curve to a protein would correspond to binding to ionizable or polar groups, and that the steep increase in the curve would be reached with binding on loose sites at the surface. In this view, the relative strength of the water association sites would decrease in this order: proton channel, lipid headgroups, BR loops in the interbilayer space.

3. What is the relationship between dynamical transitions and "melting" of associated water? Our data revealed three different dynamical transitions: one at ~150 K, which exists even in the dry sample; one at ~250 K (above which motions SA become hydration-dependent); and one at ~270 K, where motions HA_2 appear at 93% r.h. We considered the hypothesis that these transitions were related to the melting of bound water: the tighter the binding, the lower the melting point. Loosely bound water would present a melting temperature of ~270 K. For strongly bound water, existing even in "dry" PM, melting would occur at much lower temperatures, close to 170 K (Mayer, 1994). This could well correspond to the dynamical transition observed at ~150 K. The intermediate transition temperature (250 K) could correspond to water bound with intermediate strength on the surface sites of PM.

In summary, the observed motions in PM can be described as follows. Below 150 K, movements are exclusively harmonic, of low mean-square amplitude and independent of hydration; at 150 K, strongly bound water (in the proton channel?) melts, and some nonharmonic movements appear (HA_1). At ~250 K, water loosely bound to surface sites (around lipid headgroups?) melts, triggering anharmonicity in motions SA; this fits well with the observation by Fitter et al. (1997a) that BR in a delipidated PM appears as much more "rigid" than in the natural membrane, and that this difference is accentuated with increasing hydration. At

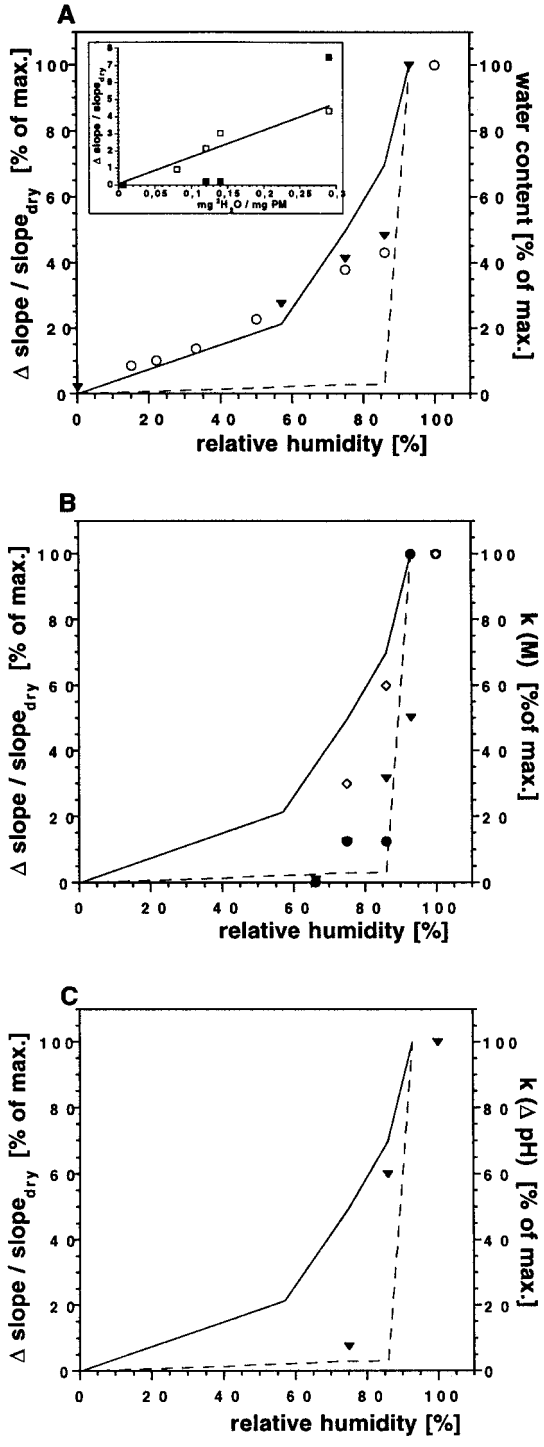

FIGURE 6 Correlation among dynamics in PM, water content, and kinetic rate constants of photocycle and pH changes (see text). Hydration-induced BR motions are represented as in Fig. 4 by the values of Δslope/slope$_{dry}$ (*solid line:* motions SA; *dotted line:* motions HA). All data (except inset in *A*) are represented as a percentage of their maximal value (obtained at either 93% or 100% r.h.); only the series of data for which the tested hydration levels reached at least 93% r.h., a hydration level at which there is almost no difference in structure and function between hydrated PM films and PM in solution (Váró and Lanyi, 1991b), is considered here. (*A*) Comparison with the water content of the sample (same symbols as in Fig. 5). *Inset:* Δslope/slope$_{dry}$ plotted against water content of the sample, showing the good correlation between motions SA (*open symbols*) and water content. (*B*) Comparison with the kinetic rate constants of the M intermediates in the photocycle. *Triangles:* rate constant for the $M_1 \Rightarrow M_2$ transition (constant $k_{M1/M2}$, Váró and Lanyi, 1991a); *circles:* rate constant for the $M_2 \Leftrightarrow N$ transition (constant $k_{M2/N}$, Váró and Lanyi, 1991a); *diamonds:* kinetic constant of M formation (taken as the reciprocal of the time to reach maximal absorbance at 407 nm in Thiedemann et al., 1992). (*C*) Comparison with the kinetics of pH changes (taken as the reciprocal of the time to reach maximal pH changes in Thiedemann et al., 1992).

270 K, melting of water in the interlamellar space liberates the final fluidity of the system, and much higher mean-square amplitude motions are observed (HA_2). Réat et al. (1998) have reported that the dynamical transition at 270 K did not appear when selectively observing the retinal pocket + extracellular half of BR, suggesting that motions HA_2 are essentially due to the cytoplasmic half of the protein and/or external loops.

Fig. 6 *A* compares the different responses of the motions SA and HA (via Δslope/slope$_{dry}$) and the water content of the sample with r.h. The values for motions SA increase proportionally with the water content. In contrast, the values for motions HA are close to zero except for very high water content. This shows that a small increase in water content triggers a proportional increase in the mean-square amplitude of motions SA. Population HA, which is nonharmonic even in the dry state, requires almost maximum hydration for the second dynamical transition to occur and large mean-square amplitudes of motions to be reached. These observations strengthen the view of the PM as a dynamical heterogeneous ensemble of populations with specifically defined characteristics.

Fig. 6 *B* shows data of the dependence on r.h. of motions SA and HA, reproduced from Fig. 4 (Δslope/slope$_{dry}$), together with data relative to rate constants of the photocycle (Váró and Lanyi, 1991a; Thiedemann et al., 1992). The rate constants calculated by Váró and Lanyi (1991a) were derived from the measured time-dependent concentrations of the photointermediates, assuming a single photocycle model. Two rate constants appeared to be clearly hydration-dependent, and both involve the intermediates M: the irreversible step between $M_1 \Rightarrow M_2$ (rate constant $k_{M1/M2}$ in Váró and Lanyi, 1991a) and the reversible step $M_2 \Leftrightarrow N$ (rate constant $k_{M2/N}$). The rate constant of M formation derived from Thiedemann et al. (1992) was calculated here as the reciprocal of the time to reach maximal absorbance at 407 nm. Fig. 6 *B* shows a strong similarity between the hydration-dependent increase of the Δslope/slope$_{dry}$ values for nonharmonic motions on the one hand, and of the kinetic constants of the M-related intermediates of the photocycle on the other. It is noteworthy that structural changes in BR occur at the level of the M_1 to M_2 transition, and that they have only been observed at relative humidities of 75% r.h. and above (Weik et al., 1998; Sass et al., 1997). The transition between these two intermediates is largely slowed down by decreasing hydration from 100% to 65% r.h. (Váró and Lanyi, 1991a). For a hydration state lower than 60% r.h., an intramolecular return of the proton from Asp-85 to the Schiff base has been detected (Váró and Lanyi, 1991a).

Furthermore, it has been reported that reprotonation of the Schiff base in fully hydrated PM samples occurs only at temperatures higher than 260 K, as in the normal sequence assumed for proton pumping, and that, as a consequence, proton pumping is inhibited (Ormos, 1991; Ormos et al., 1992). This observation might, in the present context, be correlated with the second transition to high nonharmonic amplitudes appearing for 93% r.h. at 270 K (Fig. 2).

In Fig. 6 *C* we compare our data with BR "pump activity" kinetics as a function of hydration state (Thiedemann et al., 1992). The authors measured the absorbance change of a pH indicator in the bulk phase around PM. Although these pH changes are not a direct measure of the "proton pumping" rate (defined as the proton transfer from the cytoplasmic to the extracellular side of the membrane, and which can be measured by surface-bound pH indicators, see Heberle and Dencher, 1992), their hydration dependence is likely to reflect that of the "proton pumping." As a measure of the rate of pH change, we took the reciprocal of the time to reach maximal pH change. Fig. 6 *C* shows that this rate decreases by lowering hydration of the PM samples in a way similar to the decrease of the thermal motion parameters under the same conditions.

From the present results strong correlations are observed 1) between the water content of the sample and nonharmonic movement parameters for population SA; and 2) between the nonharmonic movements (especially those of high amplitude, HA), and the kinetic constants of the M-related intermediates of the photocycle and of the proton pumping. In all cases, a change of a factor of 2 in the mean-square amplitude corresponds to a change in the rate parameters of a factor of at least 100 and often above 1000 (Korenstein and Hess, 1977; Váró and Lanyi, 1991a). The "fast" (nanosecond-to-picosecond) thermal motions therefore appear essential for the "slower" (millisecond) relaxations underlying spectral changes, proton pumping events, and conformational changes. Incoherent neutron scattering is clearly an appropriate approach to characterize the thermal motions that "serve as the lubricant that makes possible larger-scale displacements [. . .] on a physicological time scale" (Brooks et al., 1988).

The authors thank the ILL for the use of test time on IN13, especially its director, A. Leadbetter, for permission, and A. Heidemann and J. F. Barthelemy for skillful and friendly scientific and technical assistance. U.L. received a grant from the Collège Franco-Allemand.

REFERENCES

Andreani, C., A. Filabozzi, F. Menzinger, A. Desideri, A. Deriu, and D. Di Cola. 1995. Dynamics of hydrogen atoms in superoxide dismutase by quasielastic neutron scattering. *Biophys. J.* 68:2519–2523.

Bée, M. 1988. Quasielastic Neutron Scattering: Principles and Applications in Solid State Chemistry, Biology and Material Science. Adam Hilger, Bristol, UK.

Brooks, C. L. III, M. Karplus, and B. M. Pettitt. 1988. Proteins: a theoretical perspective of dynamics, structure, and thermodynamics. *In* Advances in Chemical Physics, Vol. LXXI. I. Prigogine and S. A. Rice, editors. John Wiley & Sons, New York. 94–95.

Cao, Y., G. Váró, M. Chang, B. Ni, R. Needleman, and J. K. Lanyi. 1991. Water is required for the proton transfer from Aspartate-96 to the bacteriorhodopsin Schiff base. *Biochemistry*. 30:10972–10979.

Cupane, A., M. Leone, E. Vitrano, L. Cordone, U. R. Hiltpold, K. H. Winterhalter, W. Yu, and E. E. Di Iorio. 1993. Structure-dynamic-function relationships in Asian elephant (*Elephans maximus*) myoglobin. An optical spectroscopy and flash photolysis study on functionally important motions. *Biophys. J.* 65:2461–2472.

Cusack, S. 1988. Low frequency dynamics of proteins studied by inelastic neutron scattering. *In* The Enzyme Catalysis Process: Energetics, Mechanism and Dynamics. A. Cooper, J. L. Houben, and L. C. Chien, editors. NATO ASI Series, Plenum Press, New York. 103–122.

Doster, W., S. Cusack, and W. Petry. 1989. Dynamical transition of myoglobin revealed by inelastic neutron scattering. *Nature*. 337: 754–756.

Ferrand, M., A. J. Dianoux, W. Petry, and G. Zaccaï. 1993. Thermal motions and function of bacteriorhodopsin in purple membranes: effects of temperature and hydration studied by neutron scattering. *Proc. Natl. Acad. Sci. USA.* 90:9668–9672.

Fitter, J., R. E. Lechner, and N. A. Dencher. 1997a. Influence of lipids on the dynamical behavior of bacteriorhodopsin in the purple membrane. *In* Biological Macromolecular Dynamics. S. Cusack, H. Büttner, M. Ferrand, P. Langan, and P. Timmins, editors. Adenine Press, Schenectady, NY. 123–127.

Fitter, J., R. E. Lechner, and N. A. Dencher. 1997b. Picosecond molecular motions in bacteriorhodopsin from neutron scattering. *Biophys. J.* 73: 2126–2137.

Fitter, J., R. E. Lechner, N. A. Dencher, and G. Büldt. 1996. Internal molecular motions of bacteriorhodopsin: hydration-induced flexibility studied by quasielastic incoherent neutron scattering using oriented purple membranes. *Proc. Natl. Acad. Sci. USA.* 93:7600–7605.

Glaeser, R. M., J. S. Jubb, and R. Henderson. 1985. Structural comparison of native and deoxycholate-treated purple membrane. *Biophys. J.* 48: 775–780.

Grigorieff, N., T. A. Ceska, K. H. Downing, J. M. Baldwin, and R. Henderson. 1996. Electron crystallographic refinement of the structure of bacteriorhodopsin. *J. Mol. Biol.* 259:393–421.

Heberle, J., and N. A. Dencher. 1992. Surface-bound optical probes monitor proton translocation and surface potential changes during the bacteriorhodopsin photocycle. *Proc. Natl. Acad. Sci. USA.* 89:5996–6000.

Kamikubo, H., O. Toshihiko, Y. Inamoto, F. Tokunaga, J. K. Lanyi, and M. Kataoka. 1997. The last phase of reprotonation switch in bacteriorhodopsin: the transition between the M-type and the N-type protein conformation depends on hydration. *Biochemistry*. 36: 12282–12287.

Korenstein, R., and B. Hess. 1977. Hydration effects on the photocycle of bacteriorhodopsin in thin layers of purple membrane. *Nature*. 270: 184–186.

Lechner, R. E., N. A. Dencher, J. Fitter, and T. Dippel. 1994. Two-dimensional proton diffusion on purple membrane. *Solid State Ionics*. 70/71:296–304.

Lechner, R. E., J. Fitter, N. A. Dencher, and T. Hauss. 1998. Dehydration of biological membranes by cooling: an investigation on the purple membrane. *J. Mol. Biol.* 277:593–603.

Loncharich, R. J., and B. R. Brooks. 1990. Temperature dependence of dynamics of hydrated myoglobin: comparison of force-field calculations and neutron scattering data. *J. Mol. Biol.* 215:439–455.

Mayer, E. 1994. Hyperquenched glassy bulk water: a comparison with other amorphous forms of water, and with vitreous but freezable water in a hydrogel and on hydrated methemoglobin. *In* Hydrogen Bond Networks. M. C. Bellisent-Funel and J. C. Dore, editors. Kluwer Academic Publishers, The Netherlands. 355–372.

O'Brien, F. E. M. 1948. The control of humidity by saturated salt solutions. *J. Sci. Instr.* 25:73–76.

Oesterhelt, D., and G. Krippahl. 1983. Phototropic growth of halobacteria and its use for isolation of photosynthetically deficient mutants. *Ann. Microbiol. Inst. Pasteur*. 134B:137–150.

Oesterhelt, D., and W. Stoeckenius. 1974. Isolation of cell membrane of *Halobacterium halobium* and its fractionation into red and purple membrane. *Methods Enzymol.* 31:667–678.

Ormos, P. 1991. Infrared spectroscopic demonstration of a conformational change in bacteriorhodopsin involved in proton pumping. *Proc. Natl. Acad. Sci. USA.* 88:473–477.

Ormos, P., K. Chu, and J. Mourant. 1992. Infrared study of the L, M, and N intermediates of bacteriorhodopsin using the photoreaction of M. *Biochemistry*. 31:6933–6937.

Papadopoulos, G., N. A. Dencher, G. Zaccaï, and G. Büldt. 1990. Water molecules and exchangeable hydrogen ions at the active centre of bacteriorhodopsin localized by neutron diffraction: elements of the proton pathway. *J. Mol. Biol.* 214:15–19.

Parak, F., M. Fischer, J. Heideneier, M. Engelhard, K.-D. Kohl, B. Hess, and H. Formanek. 1990. Investigation of the dynamics of bacteriorhodopsin. *Hyperfine Interact.* 58:2381–2386.

Pebay-Peyroula, E., G. Rummel, J. P. Rosenbusch, and E. M. Landau. 1997. X-ray structure of bacteriorhodopsin at 2.5 Angstroms from microcrystals grown in lipidic cubic phases. *Science*. 277:1676–1681.

Rasmussen, B. F., A. M. Stock, D. Ringe, and G. A. Petsko. 1992. Crystalline ribonuclease A loses function below the dynamical transition at 220 K. *Lett. Nat.* 357:423–424.

Réat, V., G. Zaccaï, M. Ferrand, and C. Pfister. 1997. Functional dynamics in purple membrane. *In* Biological Macromolecular Dynamics. S. Cusack, H. Büttner, M. Ferrand, P. Langan, and P. Timmins, editors. Adenine Press, Schenectady, NY. 117–121.

Réat, V., H. Patzelt, M. Ferrand, C. Pfister, D. Oesterhelt, and G. Zaccaï. 1998. Dynamics of different parts of bacteriorhodopsin: H-^{2}H exchange and neutron scattering. *Proc. Natl. Acad. Sci. USA.* 95:4970–4975.

Rogan, P. K., and G. Zaccaï. 1981. Hydration in purple membrane as a function of relative humidity. *J. Mol. Biol.* 145:281–284.

Rousso, I., N. Friedman, A. Lewis, and M. Sheves. 1997. Evidence for a controlling role of water in producing the native bacteriorhodopsin structure. *Biophys. J.* 73:2081–2089.

Rupley, J. A., and G. Careri. 1991. Protein hydration and function. *Adv. Protein Chem.* 41:37–172.

Sass, H. J., I. W. Schachowa, G. Rapp, M. H. J. Koch, D. Oesterhelt, N. A. Dencher, and G. Büldt. 1997. The tertiary structural changes in bacteriorhodopsin occur between M states: x-ray diffraction and Fourier transform infrared spectroscopy. *EMBO J.* 16:1484–1491.

Schulenberg, P. J., W. Gärtner, and S. E. Braslavsky. 1995. Time-resolved volume changes during the bacteriorhodopsin photocycle: a photothermal beam deflection study. *J. Phys. Chem.* 99:9617–9624.

Smith, J. C. 1991. Protein dynamics: comparison of simulations with inelastic neutron scattering. *Q. Rev. Biophys.* 24:227–291.

Thiedemann, G., J. Heberle, and N. A. Dencher. 1992. Bacteriorhodopsin pump activity at reduced humidity. *In* Structures and Functions of Retinal Proteins. J. L. Rigaud, editor. John Libbey Eurotext Ltd., Montrouge, France. 217–220.

Váró, G., and L. Keszthelyi. 1983. Photoelectric signals from dried oriented purple membranes of *Halobacterium halobium*. *Biophys. J.* 43: 47–51.

Váró, G., and J. K. Lanyi. 1991a. Distortions of the photocycle of bacteriorhodopsin at moderate dehydration. *Biophys. J.* 59:313–322.

Váró, G., and J. K. Lanyi. 1991b. Thermodynamics and energy coupling in the bacteriorhodopsin photocycle. *Biochemistry*. 30:5016–5022.

Weik, M., G. Zaccaï, N. A. Dencher, D. Oesterhelt, and T. Hauss. 1998. Structure and hydration of the M-state of the bacteriorhodopsin mutant D96N studied by neutron diffraction. *J. Mol. Biol.* 275:625–634.

Zaccaï, G. 1987. Structure and hydration of purple membrane in different conditions. *J. Mol. Biol.* 194:569–572.

Zaccaï, G., and D. J. Gilmore. 1979. Areas of hydration in the purple membrane of *Halobacterium halobium*: a neutron diffraction study. *J. Mol. Biol*. 132:181–191.